Marine Geology
September 2019, Volume 415 Pages 105965 (13p.)
https://doi.org/10.1016/j.margeo.2019.105965
https://archimer.ifremer.fr/doc/00502/61328/

Factors controlling frequency of turbidites in the Bengal fan during the last 248 kyr cal BP: Clues from a presently inactive channel

Fauquembergue K. [1,*], Fournier L [1], Zaragosi S. [1], Bassinot F. [2], Kissel C. [2], Malaizé B. [1], Caley T. [1], Moreno E. [3], Bachelery P. [4]

[1] UMR CNRS 5805 EPOC, Université de Bordeaux, Bâtiment B18, 33615 Pessac Cedex, France
[2] Laboratoire des Sciences du Climat et de l'Environnement (LSCE/IPSL), UMR 8212 CNRS-CEA-UVSQ, Avenue de la Terrasse, 91198 Gif-sur-Yvette Cedex, France
[3] TOTAL SA, Direction Exploration/Division Projets Nouveaux, Département Bassins et Thématiques Frontières, Tour Coupole, 2 Place Jean Millier, La Défense 6, 92078 Paris La Défense Cedex, France
[4] Université Clermont Auvergne, CNRS, IRD, OPGC, Laboratoire Magmas et Volcans, F-63000 Clermont, Ferrand, France

* Corresponding author : K. Fauquembergue, email address : kelly.fauquembergue@gmail.com

Abstract :

The seafloor of the Bay of Bengal is covered by thick sediment deposits that constitute the largest turbiditic system in the world. This system is fed primarily by the Ganges and Brahmaputra rivers, which drain the high Himalayan ranges. Sediment transfers from the delta to the deep-sea fan take place as turbidity currents in channel-levee systems. Previous studies have shown that, during high sea-level stand periods, the sediments were being mainly stored in the Ganges-Brahmaputra delta, and turbiditic transfer was occurring through active channels. Most of these channels are now inactive and sealed by hemipelagic deposits. However, the evolution of the inactive channels during the last sea-level variations has never been described in detail. Sedimentation in the currently active channel, the Active Valley, was particularly important during the last sea-level rise, which suggests a very good connection between the fluvial systems and the deep turbidite system at this time. During the MONOPOL cruise (2012), we retrieved a giant piston core (MD12-3412) near the currently inactive E4 channel. Previous studies have hypothesized that this channel is connected to the Swatch of No Ground canyon on the upper fan. The upper part of the core covers the last ~250 kyr. It reveals that, contrary to what is known about the Active Valley, the turbidite activity in E4 took place mainly during low sea-level phases (glacial stages), and stopped around 11.8 kyr cal BP. This different mode of activity suggests that (i) E4 was not abandoned but served as a secondary channel, and (ii) that the supply of turbidite material at the site of core MD12-3412 was not related to past changes in summer monsoon strength. Periods of activation of the E4 channel observed on core MD12-3412 were previously identified on the shelf area, by Hubscher and Spiess (2005), as thick Forced Regression System Tracts (FRST) after a displacement of deltaic edifices. High turbidites record on the deep basin are mainly synchronous with sea-level fall and rise conditions, but mostly during low sea-level periods. This could be explained by a residual connection between the coastal system and the E4 channel during sea level low stands.

Highlights

► A supposed inactive channel-levee since 125 kyr is investigated on the Bay of Bengal. ► The channel is reactivated mainly during low sea level stages. ► Channel activity does not seem linked with monsoons intensity but sea level variation.

Keywords : Turbidites, Bay of Bengal, Bengal fan, Sea-level, Monsoons

1. Introduction

Many high-discharge river outlets are connected to deep-sea channel-levee systems. Therefore, studies focusing on the deep-sea channel-levee formation may help to retrace paleoclimate features, such as discharge variabilities due to rainfall-increased intensities. Covault et al. (2010) demonstrated that El Niño oscillations in southern California were clearly recorded by fluvial discharges of the Santa Ana River that bypasses the New Port submarine canyon. Long-term records sometimes enable us to record sea-level variations in the form of channel-activity cyclicities (Harris et al., 2018). The combined study of turbidites sedimentology and frequency allows for the possibility of correlating channel activity and the main factors that control it. Toucanne et al. (2012), who linked the turbidite activity in the Armorican margin with the European ice-sheets melting phases, efficiently used this approach. The same approach has been also used by Prins et al. (2000) and Bourget et al. (2013, 2010), who showed that the Makran turbidites system activity and the Indus turbidite activity seem both conditioned by continental climate as well as by the sea level. This methodology was applied to the Bengal turbidite system by Fournier et al. (2017) for the Holocene turbidite activity of the Active Valley. Ganges and Brahmaputra rivers have one of the most important sedimentary discharges in the world (1x109 t/an, Milliman and Syvitski, 1992). This discharge reaches a seasonal maximum associated to heavy rains of the Indo-Asian summer monsoon (June to September; Saraswat et al., 2014). Monsoon rainfall activity results from the massive ocean-land water vapor transfer driven by the cross-equatorial pressure gradient between the Asian continent and the south Indian Ocean in response to summer insolation (Mohtadi et al., 2016). On a millennial time-scale, the link between the sediment supply and the monsoon activity is evidenced in the delta by a maximum sedimentary supply during the early Holocene (from 11ka to 7 ka; Goodbred and Kuehl, 2000), which was a climatic optimum period characterized by a peak in orbitally-driven boreal summer insolation. Most of the sediment transfers from the delta to the deep-sea Bengal fan takes place through a complex array of channel/levee systems, which constitute the largest turbidite system in the world: the Bengal fan (Figure 1; Curray et al., 2003). However, most of those channels are considered inactive today (Curray et al., 2003).

Recent system activity consists of frequent avulsions of the active canyon, the Active Valley (AV; cycle of ±750 yr; Schwenk et al., 2003). Morphological studies carried out by Hubscher et al. (1997), who focused on the channel and levee structures of the middle and lower fans, showed that the AV mostly developed during the last late glacial after the last main avulsion. Kolla et al. (2012) studied the detailed morphology of channel curves located in the upper fan, and concluded that the channel activity terminated about 6 ka BP. Weber et al. (1997) demonstrated that only the inner levee of the AV records a potential control from the monsoonal activity. Fournier et al. (2017) provided new insights about the main forcings that have affected the activity of the AV during the Holocene. They proved that monsoonal variability is not the only factor controlling the AV activity.

The distance of the core relative to the main axis of the targeted channel has an impact on the sediment section thickness and, therefore, on the time window covered by the core. The further away from the channel, the thinner the sedimentary sequence is and, consequently, the older the period we can reach with a given corer length. Thus, because cores are often located close to canyons axis, little is known about the sedimentary activity in this area during the periods preceding the Holocene. In order to address this question, inactive channels have been sampled during the 2012-MONOPOL cruise. Our study is focused on a core collected in the middle fan, on the western levee of the inactive E4 channel (the fourth channel located east of the AV; Curray et al., 2003). This core is far enough from the canyon axis to obtain the record of the activity in the last ~250 kyr BP. We propose to retrace the history of turbidites in of the E4 channel, considered as initiated and avulsed during the last 248 kyr (Curray et al., 2003). Our study of core MD12-3412, focusing on the analysis of turbidite frequency over the last ~ 250 kyr BP. This core was previously investigated by Joussain et al. (2016) that focused on the origin of detrial material. Results will then be compared with those obtained for the Holocene period on the MD12-3417 core: this core was collected on the Active Valley levee and previously studied by Fournier et al. (2017) with a similar approach.

2. Previous studies

During the Holocene, the discharge of the Ganges-Brahmaputra river reflects the regional climatic forcing: the largest sedimentation rates are observed on the continental margin during high monsoon intensity periods (Goodbred and Kuehl, 2000). Sediments eroded from the main river catchments form the largest subaerial delta of the world (Goodbred et al., 2003). This delta plays a key role in the connection between riverine sediment supplies and the deep-sea Bengal fan system. This fan system evolves through time as a result of the interaction between sea level changes and monsoon-related sediment supply, inducing variations in sedimentation rates, in accommodation space, and in the location of the major site of deposition (Umitsu, 1993; Blum et al., 2018). The monsoon-related sedimentation is evidenced, for instance, in the peak of the accumulation rates of lithogenic material on the Mahanadi basin margin (south of Ganges-Brahmaputra system; Figure 1) during the Holocene (Phillips et al., 2014). As far as the glacio-eustatism is concerned, its impact on sedimentation on the nearby Bangladesh shelf is readily seen on seismic records, which display both thick Forced Regression System Tracts (FRST) and thin transgressive system tracts (Hubscher and Spiess, 2005). The northern Bengal shelf extends over 200 km seaward, and the shelf-break is located at around 120 m depth, and can reach 170 m along its main canyon edge, i.e. The Swatch of No Ground (SoNG). As a result, most of the shelf can be exposed during the glacial maxima, resulting in a major impact of the sea level on sediment transfer from the shelf to the deep sea (Miller et al., 2005). From 20 to 29% of the total river load can reach the SoNG in the modern configuration (Michels et al., 2003), making this canyon the main connection between the deltaic edifices and the deep sea fan. When sediments leave the SoNG, they reach the upper continental slope and travel deeper through deep-sea channels as turbidity currents (Kottke et al., 2003). Deliveries from the Ganges-Brahmaputra can travel more than 1400 km in the Bengal turbidites system (Blum et al., 2018). The AV (Figure 1) is supposed to be the only channel connected to the SoNG during the Holocene. Nowadays, every clayey discharge from the Ganges-Brahmaputra that bypasses the shelf is therefore supposed to flow into the AV (Weber et al., 1997; Fournier et al., 2017). However, the entire system evolution through the Pleistocene and the

Holocene is difficult to reconstruct, mainly due to the frequent avulsions of the active channels (Curray et al., 2003).

Indeed, channels other than the AV are supposed to have been abandoned over the last 125 kyr, even if during the Pleistocene river mouths and coast lines could reach the shelf break and reactivate several canyons and multiple channels (Curray et al., 2003; Clemens et al., 2016). A few studies managed to identify Pleistocene turbidite activities on the distal fan (e.g. Kessarkar et al., 2005). However, in the upper and the middle fan, past turbidite activity has not been studied yet. Moreover, many studies focused on past channel activity using seismic data (Curray and Moore, 1971, 1974; Hubscher et al., 1997; Thu et al., 2001; Curray et al., 2003; Kolla et al., 2012) or sediment physical properties (Weber et al., 2003). Only the study by Fournier et al. (2017) utilized direct grain size measurements and geochemistry methods to decipher past changes in the turbidite frequency in the AV. Here we try to focus on the E4 channel (Figure 1) using precise measurements performed on core MD12-3412, which was recovered from its western levee.

3. Material and methods

3.1 Imagery

The echosounder Thomson Seafalcon 11 was used to acquire the bathymetry during the MONOPOL cruise of the *R.V. Marion Dufresne* (2012; 12 kHz carrier; 80 to 11000 m depth). The echosounder also included a sub-bottom profiler (3.75 kHz; ±0.31 m; Figure 2).

Other authors (Curray and Moore, 1971, 1974; Thu et al., 2001; Curray et al., 2003; Weber et al., 2003; Schwenk et al., 2003; Thomas et al., 2012; Kolla et al., 2012) precisely described each channel of the Bengal fan, and the compilation of those data (Figure 1) leads to a precise channel location.

3.2 Sediment core

The giant piston core MD12-3412 (Calypso corer, 18°18.62'N, 89°34.26'E, 2367 m water depth, 32 m long; Figure 2) has been collected in the northern Bay of Bengal, in the upper part of the middle fan during the MONOPOL cruise. As already noticed by different studies, the Calypso corer can lead to oversampling of the upper sedimentary section due to cable rebound (Skinner and McCave, 2003). Despite being now operated with a stiffer coring cable and being set up with a longer piston cable loop in order to dissipate much of the elastic rebound during coring, a slight oversampling took place in the upper ~10 m of core MD12-3412. This was highlighted and corrected by comparing the volume low-field magnetic susceptibility of this core with that of the twin gravity core (CASQ core MD12-3411Q, 9 m long). The depths of the upper sections were corrected and a composite depth was constructed for core MD12-3412. Thus, core depths used in this work are "composite depths".

3.3 Sediment laboratory analyses

The core was analyzed with the SCOPIX X-ray image-processing tool at EPOC lab (Bordeaux).

Semi-quantitative analyses of chemical elements were obtained through a XRF Core Scanner (AVAATECH) at EPOC laboratory. A step of 1 cm has been used along the entire core length to study the ratios Zr/Rb and Si/Al (Figures 3 and 4).

For the grain size, 1887 samples were collected along core MD12-3412. The measurements were performed by a Malvern Mastersizer particle size analyzer. Grain size data were visualized with a MatLAB® program to map the repartition percentage of the grain size fractions (Figure 4). Grain size distribution is presented on Figures 3 and 4, together with a grain size map. The sampling resolution varied from 0.5 cm for sequences that presented grain size variation to 5 cm for intervals that do not present significant grain size variation.

Sediment sieving and washing (over 63 µm and 150 µm mesh-sieves), thin sections, and sediment smears slides (Figure 5) were realized on core MD12-3412, in order to analyze the composition of the grains. P-wave velocities and magnetic susceptibilities (Figure 4) were measured every 2 cm on board the R.V. Marion Dufresne during the MONOPOL cruise with a Geotek multi-sensor track. The volume low-field magnetic susceptibility was measured every 2 cm on u-channels using an MS2B Bardington sensor with a 4.5 cm resolution (LSCE, Gif-sur-Yvette).

Radiocarbon dates were acquired by the ARTEMIS Accelerator Mass Spectrometry facility at the CEA center of Saclay (Gif-Sur-Yvette), and converted into calendar ages using the MARINE 13 curve (Reimer et al., 2013), that corrects the 400 yr standard reservoir age, usually used in the Bay of Bengal (Dutta et al., 2001; Southon et al., 2002). The age model (Figure 6) has been established using the R software package Clam (version 2.2; Blaauw, 2010) with a linear interpolation method at 0.1 cm resolution.

Isotopic analyses of $\delta^{18}O$ and $\delta^{13}C$ (Figures 3 and 4) were performed on the shells of planktonic foraminifera *Globigerinoides ruber sensu stricto*, *G. trilobus* and *G. sacculifer*. The sampling resolution varied from 1 cm (last climatic cycle) to 20 cm in the deepest interval downcore (Figure 4). The analyses were performed at LSCE laboratory using an ISOPRIME mass spectrometer, and converted to PDB values using a laboratory standard calibrated relative to the international National Bureau of Standards (NBS19). The internal reproducibility estimated from replicate analyses of the laboratory standard was ±0.06‰ for $\delta^{18}O$ (1 sigma).

The composition of the oxides of a tephra layer found at 5.08 m depth in the core was analysed by WDS electron microprobe CAMECA SX100 at Clermont Auvergne University (Laboratoire Magmas et Volcans - Clermont-Ferrand, France).

3.4 Stratigraphy and age model

The stratigraphy of core MD12-3412 composite was established thanks to three different kinds of proxies (Figure 6):

- Tephrochronology. Due to its oxides composition (Table 1) compared with Matthews et al. (2012) and Schulz et al. (2002) data, a tephra layer found at 506 cm depth was clearly identified as originating from the Toba eruption dated at ~73.7 ± 0.3 kyr (Mark et al., 2017).
- Radiocarbon dates. The chronology of the upper part of our composite record was based on 7 radiocarbon dates obtained from foraminifera bulk tests picked from clayey hemipelagic horizons (Table 2).
- $\delta^{18}O$ PDB. Two models were established: one using $\delta^{18}O$ PDB values of samples collected exclusively on *G. ruber* from hemipelagic intervals, and another based on more numerous samples without discriminating the origin of the sequences. Records show no significant difference, especially at our study scale (periods of 5 kyr). Thus, the stratigraphy and age model were established without correcting for the small turbidite layers.

Beyond the ^{14}C dated interval, the chronology was derived by tuning the Lisiecki and Raymo (2005) $\delta^{18}O$ PDB record to an empirical target function developed from the simple non-linear model of Imbrie and Imbrie (1980), forced by summer boreal insolation. A similar approach was followed by Bassinot et al. (1997), Lisiecki and Raymo (2005), and Shackleton et al. (1990) to develop Pleistocene age models of reference isotopic records. The two parameters of the model (T_m, i.e. the mean time constant, and b, i.e. the nonlinearity coefficient) were adjusted to ensure the best possible fit between the estimated target curve and the $\delta^{18}O$ stratigraphy of the upper part of MD12-3412, which was dated based on the seven ^{14}C tie-points and the Toba layer at 73.7 ± 0.3 kyr (Young Toba Tuff; Mark et al., 2017). The model adjustment resulted in T_m being set to 9 ka, and b set to 0.2. This approach assumed that, over several Glacial/Interglacial cycles, there existed a constant phase-lock of climatic response embedded in the $\delta^{18}O$ record of core MD12-3412 (including the monsoon signal that affected past changes in changes of $\delta^{18}O$ in regional seawater) relative to insolation forcing.

Based on the correlation with the target template modified from Imbrie and Imbrie (1980), the chronology of core MD12-3412 was developed down to ~13.5 m. The sedimentary record extends beyond that level, but the isotopic stratigraphy is difficult to interpret owing to possible large changes in sedimentation rates and/or hiatuses, and to a potential diagenetic overprint on the $\delta^{13}C$ record (see Results).

4. Results

Acoustic data acquired attest that core MD12-3412 is located about 30 km west from the E4 channel. Sense of sediment waves and high-amplitude reflectors, potentially beveled, observed on seismic profiles (Figure 2) highlight that the MD12-3412 is located on the western levee of the E4.

The analyses performed on core MD12-3412 reveal that the $\delta^{13}C$ of *G. ruber* fluctuates between 0.5 and 1.5‰ over the top 16 m of the core (Figures 2 and 3), and then drops down to anomalously low values (about -5‰). Very low $\delta^{13}C$ values in planktonic foraminifer shells had been observed by Garidel-Thoron et al. (2004) in a core from the western Pacific margin, and interpreted as being potentially linked to massive methane releases that could led to the depletion of foraminifer $\delta^{13}C$. Anomalously low P-wave velocities, approaching values typical of the speed of sound in the air (~600 m/s), were recorded in the bottom part of the core (Figures 2 and 3).

This core is composed of fine-grained sediment, mostly clay to silty-clayed sized particles (4-15 µm), observed on X-ray imagery as homogeneous light sequences (Figure 4). The grain size map (Figure 3) shows 91 grain size excursions to coarser silts or very fine sandy grains (31.3-62.5 µm), corresponding to dark, heterogeneous and finely laminated sequences in the X-ray imagery (Figure 4). Those excursions form thin (1 cm scale), fining-upward layers, commonly associated with planar laminations, and slightly erosional surfaces (Figure 5). Laminations are probably due to the variable energy of the currents, and may correspond to Bouma's term sequences where cross laminations (Tc; Bouma, 1962) are topped with planar laminations (Td). These coarse silt-to-clay excursions grade up to decantation fall-out clay. These excursions reach a mean thickness of ~4.5 cm and are illustrated by abrupt increasing Si/Al and Zr/Rb ratios at their base (Figure 4). Direct observations of the sediment and thin sections (Figure 5) reveal that rapid changes in these ratios correspond to sudden occurrences of detrital material (quartz, white & black mica for ~95% of total samples) and few foraminifera broken tests (~5%) above bioturbated sediment layers rich in foraminifers. In this core, an increase in Si/Al ratio illustrates the detrital supplies due to an increase of quartz grains, while Zr/Rb variations are correlated with grain size variations and continental supply (Dypvik and Harris, 2001; Wang et al., 2008).

On the deep-sea Bengal system, turbidites have a geochemical signature characterized by high Si and Zr contents. Thus, those sequences are interpreted as turbidites that interrupted the hemipelagic deposition.

The number of turbidites observed in 5 kyr time interval periods were counted in core MD12-3412 from 0 to 248 ka (from 0 to ~16 m on the composite core). Such a sub-orbital 5 kyr time-window makes it possible to reconstruct changes in turbidite frequency at a resolution enabling us to look at the glacio-eustatic oscillations and/or monsoon variations driven by low-latitude insolation changes, chiefly paced by precession. Four distinct periods of major turbidite activity of E4 channel were identified (Figure 7):

- an active phase during the glacial MIS 4-3-2, with peaks in activity reaching 4 turbidites/5 kyr, and even a peak of 5 turbidites/5 kyr during the last deglaciation, between MIS 2 and 1.

- an active phase during MIS 6, which seems continuous but with peaks that can reach 7 turbidites/5 kyr.

- an active phase during MIS 7, where the turbidite frequency does not exceed 2 turbidites/5 kyr.

- a slightly active phase during the recorded period of MIS 8, where the turbidite frequency does not exceed 1 turbidite/5 kyr.

Those 4 periods of stronger turbidite activity are separated by inactive periods during MIS 1, MIS 5, at the onset, and at the end and the beginning of MIS 7 (Figure 7). The undated base of the core shows numerous turbidites (Figure 4).

The thickness of the turbidites was measured using a combination of grain size data (difference of depth between the coarse bases and the top of the hemipelagic layers; Figures 4 and 5), geochemical data (difference of depth between the high and stable Si/Al & Zr/Rb ratios; Figure 4), and evidences of internal structures in sequences (laminations and erosive surfaces; Figure 5). Turbidites thicknesses vary from 1 to 13 cm during the activity periods. Even if the mean turbidite sizes seem greater during MIS 4-3-2 than during MIS 6, the difference is not significant (mean value of 6.22 ± 2.14 cm for

MIS 4-3-2, and 4.1 ± 3.32 cm for MIS 6). The mean value of turbidites thickness during MIS 8 is not relevant because MIS 8 is not entirely recorded.

5. Discussion

5.1 Main forcings affecting the turbidites activity

In MD12-3412, the anomalous $\delta^{13}C$ signal and p-waves velocities could be associated with a partial re-crystallization of foraminifer shells in the presence of methane during diagenetic processes. Such hypothesis is backed-up by the broad occurrence of gas hydrate areas in the Bay of Bengal (Figures 2 and 3; Dewangan et al., 2013). Anomalies are synchronous with a huge shift recorded during the MIS 8-7 on the lower fan, when the system became suddenly highly turbiditic according to the Mid-Brunhes Transition (Weber and Reilly, 2018). To address a potential problem with $\delta^{18}O$ PDB values, we will only focus on the upper part of the core, for which a precise age model could be achieved.

The presence of many sequences that exhibit finning upward associated with brutal increases of Si/Al and Zr/Rb, followed by decreases, leads to the conclusion that core MD12-3412 records fine-grained turbidites (coarse-silts or very fine-sand grain size excursions) interspersed by hemipelagic sequences (lighter silty-clays). Based on our observations, grain size excursions showing these specific features were considered as fine turbidite sequences (Figures 4 and 5). Geochemistry is well correlated with turbidite sequences, X-ray images, and grain sizes. During the last 248 kyr cal BP, three active and two inactive phases were observed on the channel.

According to Phillips et al. (2014), detrital material supplies and sedimentation rates were low during the last glacial maximum at the outlet of the Mahanadi due to the weakened SW monsoon. However, they increased during the early Holocene in association with increased monsoon activity driven by the low-latitude summer insolation maximum. Erosion of the Godavari catchment erosion (Figure 1) increased during the late Holocene due to a decrease in monsoon intensities, and could have led to an increase in sedimentation rates during this period (Giosan et al.; 2017). Some studies suggest that the summer Asian monsoon was enhanced during interglacial periods, and reduced during glacial periods (Guo et al., 2000; Sun et al., 2006). According to Clemens and Prell (2003), and Caley et al. (2011), internal climate forcing sets the timing of strong Indo-Asian summer monsoons within both the precession and the obliquity cycles. Another hypothesis, based on Chinese cave speleothem records, is that the monsoon response is nearly in phase with the summer boreal insolation (Cheng et al., 2009;

Dykoski et al., 2005; Wang et al., 2008). However, the increase in monsoon intensities during MIS 5 and 1 corresponds to inactive phase in the middle fan, while low monsoon intensities during MIS 6 and 2 correspond to high turbidite frequencies. Moreover, the sedimentation rates are slightly higher during glacial periods than in interglacial periods (Figure 62). Hypotheses considered here in driving the Indo-Asian monsoon at the orbital scale are not correlated with turbidites activity within the MD12-3412 (Figure 7). The Indo-Asian monsoon intensity is therefore not the first-order forcing that controls the turbidite activity in the middle Bengal fan and in the E4 channel at the glacial-interglacial or orbital scales. During MIS 6, the evolution of the thickness of the turbidites seems negatively correlated to the monsoons intensity (Figure 7), probably because low-intensity but frequent monsoons lead to a progressive flushing of large amounts of sediment, while high-intensity but sporadic ones lead to a strong punctual flushing. However, it is hard to establish a clear link between both records. The study of the frequencies of other low-stand turbidites in other locations of the Bengal fan would be necessary to propose monsoons as a secondary-order forcing that controls the turbidite activity in the Bay of Bengal.

Based on geochemical and mineralogical evidences, Joussain et al. (2016) concluded that detrital material at the site of core MD12-3412 was derived from the Ganges and Brahmaputra rivers during interglacial periods (MIS 5 and 1), while it derived from a mixture of material originating from the Ganges-Brahmaputra rivers and the Indo-Burman Ranges during MIS 6, 4, 3 and 2. Several major changes in the sea level have been recorded during the last 248 kyr, namely three periods of low sea level during MIS 8, MIS 6, and MIS 4-3-2, and three periods of high sea level during MIS 7, 5 and 1 (Grant et al., 2012). The main phases of turbidite activity are synchronous with both periods of low sea level and sea level fall or rise (Figure 7). The low sea level configuration promotes the connection between the rivers and the deep sea (Sijinkumar et al., 2016). During low stands, the Bangladesh shelf is subaerial due to its shallowness (<120 m depth). Oolthic beach barriers accumulated during sea-level low stands indicate that the current outer shelf was not influenced by massive terrigenous input (Wiedicke et al., 1999). Thus, the Ganges-Brahmaputra outlet is probably connected to the SoNG that incised the shelf (Figure 1). These periods (MIS 8, 6, 4-2) are recorded on the continental shelf by thick FRST sequences, extending also beyond the break of the slope for MIS 8 and 6 (Hubscher and Spiess, 2005). Low stand deposits are deltaic lobes on the continental slope, prograding during the MIS 6, and retrograding during MIS 8 and 4-3-2 (Hubscher and Spiess, 2005). The low sea level increases the area of deltaic sedimentation, and brings it closer to the Bengal fan. In fact, the greater feeding induces an increase of the turbidite activity in the Bengal fan, which is consistent with Curray et al.'s (2003) suggestion that channel/levee systems were built during periods of low sea level. The deltaic sedimentation, taking place all along the continental shelf, may explain the mixed origin of the sediments (Joussain et al., 2016) during MIS 6 and 4-3-2. Moreover, this lower sea level configuration also explained the enhanced supply found by Panmei et al. (2018) on the upper fan. The magnetic susceptibility curve relative to sediment source supply seems strongly correlated with sea level variations during the last glacial period from MIS 4 to MIS 2. Conversely, high sea level stands are characterized by the absence of turbidite activity in the upper fan (Figure 7). High stands make possible the construction of thin transgressive system tracts sequences extending on the continental shelf (Hubscher and Spiess, 2005). There is a landward shift of deltaic sedimentation during high stands (Hubscher and Spiess, 2005), which can explain why only the major rivers supplies (Ganges-Brahmaputra) can reach the upper Bengal fan (Joussain et al., 2016). Thus, the landward shift of deltaic edifice induces a decrease of turbidite activity in the middle fan recorded by the western flank of E4 (Figure 7). Those results highlighted that the turbiditic transfer to the upper fan is mainly related to the glacial – interglacial changes of sea level. During a low stand, the canyon is the main conduit, whereas during a high stand the sediment is stored in the delta.

5.2 Evolution of turbidite activity in the Bengal fan

According to Curray et al. (2003), the Quaternary upper Bengal fan is subdivided into four subfans, showing some lateral shifts in the Bay of Bengal. Two of them concern the period since 250 kyr, which was also considered in this work. The first subfan, fed between 465 and 125 kyr cal BP (before the MIS 5), is located on the eastern side of the AV, and was mainly fed by the SoNG, but with multiple sources on the platform margins (Curray et al., 2003). The modern fan configuration, with the SoNG as the only fan feeder, is considered to be in place since 125 kyr cal BP (since the MIS 5). Thus, turbidites recorded since 125 kyr cal BP are characterized by a shift in sedimentation from a channel on the east side of the fan (the E4 channel) to the AV (Curray et al., 2003). This shift is not due to a canyon shift but to a lateral channel shift around 19 °N on the upper fan (Figure 1; Curray et al., 2003). Thus, the E4 channel is supposed connected to the SoNG outlet as the AV. Glacial MIS 4-3-2 presents a lower activity than the previous glacial MIS 6, and interglacial MIS 5 does not present any activity, contrary to the previous interglacial MIS 7 that presents a low activity. Our results are consistent with a change in turbidite activity that took place around 125 kyr cal BP, but they also reveal that turbidite activity is still recorded after 125 kyr cal BP near the E4 channel during periods of regression and low sea level stand (Figure 7). The E4 was probably a rare reactivated channel during low stand, and was not completely avulsed after 125 ka, contrary to the suggestion of Curray et al. (2003). Turbidite activity recorded near the E4 channel terminated around 11.8 kyr cal BP, and hemipelagic sedimentation settled above, with a sedimentation rate around 2 cm/kyr (Figure 7).

The E4 terminated its activity around 11.8 ka cal BP, while the AV initiated around 14.5 kyr cal BP (Weber et al., 1997), and turbidite activity was highest during periods of sea level rise and during the first stages of the Holocene high stand (Weber et al., 1997; Fournier et al., 2017). This is contrary to what we observe close to the E4 channel. These two channels therefore functioned differently depending on the sea level (Figure 8). Because our data suggest that E4 channel was activated during low stands, the connection between the E4 channel and the SoNG outlet on the upper fan could still be active, meaning that the AV was not the only channel connected to the SoNG shelf during the period between 14.5 and 11.8 ka cal BP.

5.3 Comparisons with the modern Bengal configuration

Even if some discharges are recorded in the AV (Fournier et al., 2017; Figure 8), the turbidites supply shows a clear shift from a direct supply before 9.2 kyr to a more complex model with different factors involved since 9.2 kyr (Figure 8; river migrations, delta construction, and potentially anthropogenic impact). Turbidite activity in the E4 channel suggests that it has been reactivated as a secondary channel during regression, transgression, and low sea level stand periods since at least the Mid-Brunhes Transition (Figure 8; Weber and Reilly, 2018). This functioning does not seem common to every canyon and channels in the Bay of Bengal, but it has already been observed on other turbidite systems. A close but quite different functioning system was observed for the Indus system (Bourget et al., 2013). A delta formed during forced regression conditions reactivated multiple canyons and gullies that fed several channels. In our case, only the SoNG was recognized as a feeding canyon along the shelf during the last 125 kyr.

Jipa and Panin (2018) highlighted two main models explaining the functioning of modern canyons in the Black Sea: the active eastern narrow shelf canyons, and the inactive western wide shelf canyons. The wide shelf canyons are mainly active during low stand periods, while narrow shelf canyons are active during both low stand and high stand conditions. Narrow shelf canyons in the Black Sea seem to record the same kind of configuration of the Newport submarine canyon (Covault et al., 2010), while the Bengal shelf mainly belongs to the wide shelf class and presents the same features. Fluvial outlets are disconnected to the main canyon head (SoNG) during high stands, and this configuration limits the direct flushing of fluvial supply to the canyon and then to the deep-sea channel system, even during periods of high monsoon intensity.

6. Summary and conclusion

Grain size and geochemical analyses of MD12-3412 allowed for the reconstruction of the E4 channel turbidite activity in the upper part of the middle Bengal fan. The following main conclusions have been drawn from the results of the analyses:

(1) For the last 248 kyr cal BP, periods of higher turbidite activity mainly occurred during the glacial periods MIS 6 and MIS 2-3-4. These results coincide with Forced Regression System Tracts deposition periods observed on the shelf (Hubscher and Spiess, 2005), suggesting an exceptional narrow link between the sedimentary supply by-passing the shelf during glacial periods and the E4 channel activity.

(2) Sea level variations seem to be the main forcing affecting the turbiditic sedimentation in the middle part of the Bengal fan at glacial/interglacial time scale. Even if avulsion is observed in the Bengal fan (Curray et al., 2003), the E4 channel and the middle fan are reactivated during low stand periods. Thus, the E4 channel has not been abandoned and avulsed after 125 ka.

(3) A link between sea level variations and channel activity might have conditioned both the delta extent and the break slope position, similarly to what was observed for the Indus system and for the Black Sea systems. A decrease in sea level leads the delta to become subaerial, with sediments having no buffer tank and not enough accommodation space. Such configuration enables the reactivation of secondary channels, such as the E4, so as to offset this lack of space.

Acknowledgements

This work was conducted in the framework of the MONOPOL ANR project (no. ANR 2011 Blanc SIMI 5-6 024 04). We are grateful to the Institut polaire français Paul-Emile Victor (IPEV) that supported the oceanographic cruise and we are grateful to the *Marion Dufresne* crew. The Laboratoire des Sciences du Climat et de l'Environnement (LSCE), the Centre de Recherche et d'Enseignement de Géosciences de l'Environnement (CEREGE), the University of Paris-Sud, the Institut de Physique du Globe de Paris (IPGP), the Muséum National d'Histoire Naturelle (MNHN), the OPGC lab contributed to this work. We thank the 'ARTEMIS' technical platform for radiocarbon dating. We also would like to thanks the reviewers which remarks clearly improved this paper. Finally, we are also grateful to EPOC technicians and engineers: P Lebleu, I Billy, O Ther, B Martin, B Cosson, L Rossignol, and MH Castera for their help in the data acquisition.

Bibliography

Bassinot, F., Beaufort, L., Vincent, E., Labeyrie, L., 1997. Changes in the dynamics of western equatorial Atlantic surface currents and biogenic productivity at the “Mid-Pleistocene revolution” (930KA), Proceedings of the Ocean Drilling Program, Scientific Results. Ocean Drilling Program. https://doi.org/10.2973/odp.proc.sr.154.1997

Blaauw, M., 2010. Methods and code for ‘classical’ age-modelling of radiocarbon sequences. Quat. Geochronol. 5, 512–518. https://doi.org/10.1016/j.quageo.2010.01.002

Blum, M., Rogers, K., Gleason, J., Najman, Y., Cruz, J., Fox, L., 2018. Allogenic and Autogenic Signals in the Stratigraphic Record of the Deep-Sea Bengal Fan. Sci. Rep. 8. https://doi.org/10.1038/s41598-018-25819-5

Bouma, A., H., 1962. Sedimentology of some Flysch Deposits: A Graphic Approach to Facies Interpretation. Elsevier Pub. Co.

Bourget, J., Zaragosi, S., Ellouz-Zimmermann, S., Ducassou, E., Prins, M.A., Garlan, T., Lanfumey, V., Schneider, J.-L., Rouillard, P., Giraudeau, J., 2010. Highstand vs. lowstand turbidite system growth in the Makran active margin: Imprints of high-frequency external controls on sediment delivery mechanisms to deep water systems. Mar. Geol. 274, 187–208. https://doi.org/10.1016/j.margeo.2010.04.005

Bourget, J., Zaragosi, S., Rodriguez, M., Fournier, M., Garlan, T., Chamot-Rooke, N., 2013. Late Quaternary megaturbidites of the Indus Fan: Origin and stratigraphic significance. Mar. Geol. 336, 10–23. https://doi.org/10.1016/j.margeo.2012.11.011

Caley, T., Malaizé, B., Zaragosi, S., Rossignol, L., Bourget, J., Eynaud, F., Martinez, P., Giraudeau, J., Charlier, K., Ellouz-Zimmermann, N., 2011. New Arabian Sea records help decipher orbital timing of Indo-Asian monsoon. Earth Planet. Sci. Lett. 308, 433–444. https://doi.org/10.1016/j.epsl.2011.06.019

Cheng, H., Edwards, R.L., Broecker, W.S., Denton, G.H., Kong, X., Wang, Y., Zhang, R., Wang, X., 2009. Ice Age Terminations. Science 326, 248–252. https://doi.org/10.1126/science.1177840

Clemens, S.C., Prell, W.L., 2003. A 350,000 year summer-monsoon multi-proxy stack from the Owen Ridge, Northern Arabian Sea. Mar. Geol. 201, 35–51. https://doi.org/10.1016/S0025-3227(03)00207-X

Collett, T.S., Boswell, R., Cochran, J.R., Kumar, P., Lall, M., Mazumdar, A., Ramana, M.V., Ramprasad, T., Riedel, M., Sain, K., Sathe, A.V., Vishwanath, K., 2014. Geologic implications of gas hydrates in the offshore of India: Results of the National Gas Hydrate Program Expedition 01. Mar. Pet. Geol., Geologic implications of gas hydrates in the offshore of India: Results of the National Gas Hydrate Program Expedition 01 58, Part A, 3–28. https://doi.org/10.1016/j.marpetgeo.2014.07.021

Covault, J.A., Romans, B.W., Fildani, A., McGann, M., Graham, S.A., 2010. Rapid Climatic Signal Propagation from Source to Sink in a Southern California Sediment-Routing System. J. Geol. 118, 247–259. https://doi.org/10.1086/651539

Curray, J.R., Moore, D.G., 1974. Sedimentary and Tectonic Processes in the Bengal Deep-Sea Fan and Geosyncline, in: Burk, C.A., Drake, C.L. (Eds.), The Geology of Continental Margins. Springer Berlin Heidelberg, Berlin, Heidelberg, pp. 617–627. https://doi.org/10.1007/978-3-662-01141-6_45

Curray, J.R., Moore, D.G., 1971. Growth of the Bengal Deep-Sea Fan and Denudation in the Himalayas. Geol. Soc. Am. Bull. 82, 563. https://doi.org/10.1130/0016-7606(1971)82[563:GOTBDF]2.0.CO;2

Curray, J.R., Emmel, F.J., Moore, D.G., 2003. The Bengal Fan: morphology, geometry, stratigraphy, history and processes. Mar. Pet. Geol. 19, 1191–1223. https://doi.org/10.1016/s0264-8172(03)00035-7

Dewangan, P., Basavaiah, N., Badesab, F.K., Usapkar, A., Mazumdar, A., Joshi, R., Ramprasad, T., 2013. Diagenesis of magnetic minerals in a gas hydrate/cold seep environment off the Krishna–Godavari basin, Bay of Bengal. Mar. Geol. 340, 57–70. https://doi.org/10.1016/j.margeo.2013.04.016

Dutta, K., Bhushan, R., Somayajulu, B.L.K., 2001. ΔR correction values for the Northern Indian ocean 6.

Dykoski, C., Edwards, R., Cheng, H., Yuan, D., Cai, Y., Zhang, M., Lin, Y., Qing, J., An, Z., Revenaugh, J., 2005. A high-resolution, absolute-dated Holocene and deglacial Asian monsoon record from Dongge Cave, China. Earth Planet. Sci. Lett. 233, 71–86. https://doi.org/10.1016/j.epsl.2005.01.036

Dypvik, H., Harris, N.B., 2001. Geochemical facies analysis of fine-grained siliciclastics using Th/U, Zr/Rb and (Zr+ Rb)/Sr ratios. Chem. Geol. 181, 131–146.

Fournier, L., Fauquembergue, K., Zaragosi, S., Zorzi, C., Malaizé, B., Bassinot, F., Joussain, R., Colin, C., Moreno, E., Leparmentier, F., 2017. The Bengal fan: External controls on the Holocene Active Channel turbidite activity. The Holocene 27, 900–913. https://doi.org/10.1177/0959683616675938

Garidel-Thoron, T. de, Beaufort, L., Bassinot, F., Henry, P., 2004. Evidence for large methane releases to the atmosphere from deep-sea gas-hydrate dissociation during the last glacial episode. Proc. Natl. Acad. Sci. U. S. A. 101, 9187–9192. https://doi.org/10.1073/pnas.0402909101

Giosan, L., Ponton, C., Usman, M., Blusztajn, J., Fuller, D.Q., Galy, V., Haghipour, N., Johnson, J.E., McIntyre, C., Wacker, L., Eglinton, T.I., 2017. Short communication: Massive erosion in monsoonal central India linked to late Holocene land cover degradation. Earth Surf. Dyn. 5, 781–789. https://doi.org/10.5194/esurf-5-781-2017

Goodbred Jr, S.L., Kuehl, S.A., Steckler, M.S., Sarker, M.H., 2003. Controls on facies distribution and stratigraphic preservation in the Ganges–Brahmaputra delta sequence. Sediment. Geol. 155, 301–316.

Goodbred, S.L., Kuehl, S.A., 2000. Enormous Ganges-Brahmaputra sediment discharge during strengthened early Holocene monsoon. Geology 28, 1083–1086. https://doi.org/10.1130/0091-7613(2000)28<1083:egsdds>2.0.co;2

Grant, K., Rohling, E., Bar-Matthews, M., Ayalon, A., Medina-Elizalde, M., Ramsey, C.B., Satow, C., Roberts, A., 2012. Rapid coupling between ice volume and polar temperature over the past 150,000 [thinsp] years. Nature 491, 744–747.

Guo, Z., Biscaye, P., Wei, L., Chen, X., Peng, S., Liu, T., 2000. Summer monsoon variations over the last 1.2 Ma from the weathering of loess-soil sequences in China. Geophys. Res. Lett. 27, 1751–1754. https://doi.org/10.1029/1999GL008419

Harris, A.D., Baumgardner, S.E., Sun, T., Granjeon, D., 2018. A Poor Relationship Between Sea Level and Deep-Water Sand Delivery. Sediment. Geol. 370, 42–51. https://doi.org/10.1016/j.sedgeo.2018.04.002

Hubscher, C., Spiess, V., 2005. Forced regression systems tracts on the Bengal Shelf. Mar. Geol. 219, 207–218. https://doi.org/10.1016/j.margeo.2005.06.037

Hubscher, C., Spiess, V., Breitzke, M., Weber, M.E., 1997a. The youngest channel-levee system of the Bengal Fan: results from digital sediment echosounder data. Mar. Geol. 141, 125–145. https://doi.org/10.1016/s0025-3227(97)00066-2

Imbrie, J., Imbrie, J.Z., 1980. Modeling the Climatic Response to Orbital Variations. Science 207, 943–953. https://doi.org/10.1126/science.207.4434.943

Joussain, R., Colin, C., Liu, Z., Meynadier, L., Fournier, L., Fauquembergue, K., Zaragosi, S., Schmidt, F., Rojas, V., Bassinot, F., 2016b. Climatic control of sediment transport from the Himalayas to the proximal NE Bengal Fan during the last glacial-interglacial cycle. Quat. Sci. Rev. 148, 1–16. https://doi.org/10.1016/j.quascirev.2016.06.016

Kessarkar, P.M., Rao, V.P., Ahmad, S.M., Patil, S.K., Kumar, A.A., Babu, G.A., Chakraborty, S., Rajan, R.S., 2005. Changing sedimentary environment during the Late Quaternary: Sedimentological and isotopic evidence from the distal Bengal Fan. Deep-Sea Res. Part -Oceanogr. Res. Pap. 52, 1591–1615. https://doi.org/10.1016/j.dsr.2005.01.009

Kolla, V., Bandyopadhyay, A., Gupta, P., Mukherje, B., Ramana, D.V., 2012a. Morphology and Internal Structure of a Recent Upper Bengal Fan-Valley Complex, in: Prather, B.E., Deptuck, M.E., Mohrig, D., Hoorn, B.V., Wynn, R.B. (Eds.), Application of the Principles of Seismic Geomorphology to Continental-Slope and Base-of-Slope Systems: Case Studies from Seafloor and Near-Seafloor Analogues. SEPM Special Publication.

Kottke, B., Schwenk, T., Breitzke, M., Wiedicke, M., Kudrass, H.R., Spiess, V., 2003. Acoustic facies and depositional processes in the upper submarine canyon Swatch of No Ground (Bay of Bengal). Deep-Sea Res. Part Ii-Top. Stud. Oceanogr. 50, 979–1001. https://doi.org/10.1016/s0967-0645(02)00616-1

Lisiecki, L.E., Raymo, M.E., 2005. "A Pliocene-Pleistocene stack of 57 globally distributed benthic δ18O records." Paleoceanography 20, n/a-n/a. https://doi.org/10.1029/2005PA001164

Mark, D.F., Renne, P.R., Dymock, R.C., Smith, V.C., Simon, J.I., Morgan, L.E., Staff, R.A., Ellis, B.S., Pearce, N.J.G., 2017. High-precision 40Ar/39Ar dating of pleistocene tuffs and temporal anchoring of the Matuyama-Brunhes boundary. Quat. Geochronol. 39, 1–23. https://doi.org/10.1016/j.quageo.2017.01.002

Matthews, N.E., Smith, V.C., Costa, A., Durant, A.J., Pyle, D.M., Pearce, N.J.G., 2012. Ultra-distal tephra deposits from super-eruptions: Examples from Toba, Indonesia and Taupo Volcanic Zone, New Zealand. Quat. Int. 258, 54–79. https://doi.org/10.1016/j.quaint.2011.07.010

Michels, K.H., Suckow, A., Breitzke, M., Kudrass, H.R., Kottke, B., 2003. Sediment transport in the shelf canyon "Swatch of No Ground" (Bay of Bengal). Deep-Sea Res. Part Ii-Top. Stud. Oceanogr. 50, 1003–1022. https://doi.org/10.1016/s0967-0645(02)00617-3

Miller, K.G., Kominz, M.A., Browning, J.V., Wright, J.D., Mountain, G.S., Katz, M.E., Sugarman, P.J., Cramer, B.S., Christie-Blick, N., Pekar, S.F., 2005. The Phanerozoic record of global sea-level change. science 310, 1293–1298.

Milliman, J.D., Syvitski, J.P.M., 1992. Geomorphic/Tectonic Control of Sediment Discharge to the Ocean: The Importance of Small Mountainous Rivers. J. Geol. 100, 525–544.

Mohtadi, M., Prange, M., Steinke, S., 2016. Palaeoclimatic insights into forcing and response of monsoon rainfall. Nature 533, 191–199. https://doi.org/10.1038/nature17450

Phillips, S.C., Johnson, J.E., Giosan, L., Rose, K., 2014. Monsoon-influenced variation in productivity and lithogenic sediment flux since 110 ka in the offshore Mahanadi Basin, northern Bay of Bengal. Mar. Pet. Geol., Geologic implications of gas hydrates in the offshore of India: Results of the National Gas Hydrate Program Expedition 01 58, Part A, 502–525. https://doi.org/10.1016/j.marpetgeo.2014.05.007

Prins, M.A., Postma, G., Cleveringa, J., Cramp, A., Kenyon, N.H., 2000. Controls on terrigenous sediment supply to the Arabian Sea during the late Quaternary: the Indus Fan. Mar. Geol. 169, 327–349. https://doi.org/10.1016/S0025-3227(00)00086-4

Reimer, P.J., Bard, E., Bayliss, A., Beck, J.W., Blackwell, P.G., Ramsey, C.B., Buck, C.E., Hai Cheng, Edwards, R.L., Friedrich, M., Grootes, P.M., Guilderson, T.P., Haflidason, H., Hajdas, I., Hatté, C., Heaton, T.J., Hoffmann, D.L., Hogg, A.G., Hughen, K.A., Kaiser, K.F., 2013. Intcal13 and Marine13 Radiocarbon Age Calibration Curves 0-50,000 Years Cal Bp. Radiocarbon 55, 1869–1887.

Saraswat, R., Nigam, R., Correge, T., 2014. A glimpse of the Quaternary monsoon history from India and adjoining seas. Palaeogeogr. Palaeoclimatol. Palaeoecol. 397, 1–6. https://doi.org/10.1016/j.palaeo.2013.11.001

Schulz, H., Emeis, K.-C., Erlenkeuser, H., von Rad, U., Rolf, C., 2002. The Toba Volcanic Event and Interstadial/Stadial Climates at the Marine Isotopic Stage 5 to 4 Transition in the Northern Indian Ocean. Quat. Res. 57, 22–31. https://doi.org/10.1006/qres.2001.2291

Schwenk, T., Spiess, V., Hubscher, C., Breitzke, M., 2003. Frequent channel avulsions within the active channel-levee system of the middle Bengal Fan - an exceptional channel-levee development derived from Parasound and Hydrosweep data. Deep-Sea Res. Part Ii-Top. Stud. Oceanogr. 50, 1023–1045. https://doi.org/10.1016/s0967-0645(02)00618-5

Shackleton, N.J., Berger, A., Peltier, W.R., 1990. An alternative astronomical calibration of the lower Pleistocene timescale based on ODP Site 677 11.

Sijinkumar, A.V., Clemens, S., Nath, B.N., Prell, W., Benshila, R., Lengaigne, M., 2016. δ18O and salinity variability from the Last Glacial Maximum to Recent in the Bay of Bengal and Andaman Sea. Quat. Sci. Rev. 135, 79–91. https://doi.org/10.1016/j.quascirev.2016.01.022

Skinner, L.C., McCave, I.N., 2003. Analysis and modelling of gravity- and piston coring based on soil mechanics. Mar. Geol. 199, 181–204. https://doi.org/10.1016/S0025-3227(03)00127-0

Southon, J., Kashgarian, M., Fontugne, M., Metivier, B., W-S Yim, W., 2002. Marine Reservoir Corrections for the Indian Ocean and Southeast Asia. Radiocarbon 44, 167–180. https://doi.org/10.1017/S0033822200064778

Stow, D.A., Howell, D.G., Nelson, C.H., 1985. Sedimentary, tectonic, and sea-level controls, in: Submarine Fans and Related Turbidite Systems. Springer, pp. 15–22.

Sun, Y., Clemens, S.C., An, Z., Yu, Z., 2006. Astronomical timescale and palaeoclimatic implication of stacked 3.6-Myr monsoon records from the Chinese Loess Plateau. Quat. Sci. Rev. 25, 33–48. https://doi.org/10.1016/j.quascirev.2005.07.005

Thomas, B., Despland, P., Holmes, L., 2012. Submarine Sediment Distribution Patterns within the Bengal Fan System, Deep Water Bengal Basin, India; #50756 (2012) 24.

Thu, M.K., Tokuyama, H., Murayama, M., 2001. HINDOO cruise deep-sea channel survey in the Bay of Bengal. J. Geol. Soc. Jpn. 107.

Toucanne, S., Zaragosi, S., Bourillet, J.-F., Dennielou, B., Jorry, S.J., Jouet, G., Cremer, M., 2012. External controls on turbidite sedimentation on the glacially-influenced Armorican margin (Bay of Biscay, western European margin). Mar. Geol. 303–306, 137–153. https://doi.org/10.1016/j.margeo.2012.02.008

Umitsu, M., 1993. Late Quaternary sedimentary environments and landforms in the Ganges Delta. Sediment. Geol. 83, 177–186.

Wang, H., Liu, L., Feng, Z., 2008. Spatiotemporal variations of Zr/Rb ratio in three last interglacial paleosol profiles across the Chinese Loess Plateau and its implications for climatic interpretation. Sci. Bull. 53, 1413–1422. https://doi.org/10.1007/s11434-008-0068-0

Wang, Y., Cheng, H., Edwards, R.L., Kong, X., Shao, X., Chen, S., Wu, J., Jiang, X., Wang, X., An, Z., 2008. Millennial- and orbital-scale changes in the East Asian monsoon over the past 224,000 years. Nature 451, 1090–1093. https://doi.org/10.1038/nature06692

Weber, M.E., Wiedicke, M.H., Kudrass, H.R., Hubscher, C., Erlenkeuser, H., 1997b. Active growth of the Bengal Fan during sea-level rise and highstand. Geology 25, 315–318. https://doi.org/10.1130/0091-7613(1997)025<0315:agotbf>2.3.co;2

Weber, M.E., Wiedicke-Hombach, M., Kudrass, H.R., Erlenkeuser, H., 2003. Bengal Fan sediment transport activity and response to climate forcing inferred from sediment physical properties. Sediment. Geol. 155, 361–381. https://doi.org/10.1016/s0037-0738(02)00187-2

Weber, M.E., Reilly, B.T., 2018. Hemipelagic and turbiditic deposits constrain lower Bengal Fan depositional history through Pleistocene climate, monsoon, and sea level transitions. Quat. Sci. Rev. 199, 159–173. https://doi.org/10.1016/j.quascirev.2018.09.027

Wiedicke, M., Kudrass, H.-R., Hübscher, C., 1999. Oolitic beach barriers of the last Glacial sea-level lowstand at the outer Bengal shelf. Marine Geology 157, 7-18.

Table 1: Comparison between Toba eruption features (Matthews et al., 2012; Schulz et al., 2002) and the MD12-3412 tephra sequence.

	MD12-3412 samples analyses (%)	**Analyses from continental samples (%; Matthews et al., 2012)**	**Analyses from the middle fan (%; Schulz et al., 2002)**
	n=14	n=274	n=4
SiO_2	77.13 ± 0.08	76.80-77.44	78.60
TiO_2	0.068 ± 0.007	0.05-0.08	0.06
Al_2O_3	12.62 ± 0.06	12.40-12.70	12.59
FeO	0.91 ± 0.04	0.77-0.97	1.03
MnO	0.06 ± 0.02	0.06-0.08	0.06
MgO	0.062 ± 0.006	0.04-0.07	0.06
CaO	0.80 ± 0.02	0.69-0.89	0.76
Na_2O	3.14 ± 0.05	2.98-3.38	1.80
K_2O	5.20 ± 0.04	4.98-5.17	5.03
P_2O_5	0.017 ± 0.007	(unknown)	(unknown)
Tephra thickness (cm)	8	2-15	x

Table 2: Results of MD12-3412 foraminifers bulk radiocarbon datings after calibrations

Depth (cm)	**Age (yr cal BP)**	**Error (yr cal BP)**
25.8	1776	85
41.5	10738	150
78.4	13823.5	137.5
101.4	16651	241
124.3	19467	219
169.7	28327.5	334.5
205.4	31420.5	366.5

Figure 1: Location map and physiography of the Ganges-Brahmaputra sedimentary system, from the catchment to the deep-sea fan. Fluvial systems are in light blue, and channelizations of the Bengal fan according to different sources and interpretations are visible in a shade of blue. Names of each channel are from Curray et al. (2003). The inset shows an enlarged view of the upper and middle fan with the location of the core MD12-3412 and -120 m isobaths. The summary of channels morphology was reported thanks to Curray et al. (2003), Kolla et al. (2012), Kottke et al. (2003), Thomas et al. (2012), Thu et al. (2001), Weber et al. (2003).

Figure 2: Very High seismic profile and interpretation from MD12-3412 environments.

Figure 3: Interpretative log, grain size distribution (D50= Decile50 and colours illustrate the % of sieve non-passing fraction, see scale at the bottom), δ18O results for G. ruber, and position of Marine Isotopic Stages (MIS). P-waves velocities and δ13C G. ruber highlight abnormal high values below 13.80 m depth. The correlation established between MD12-3411Q and MD12-3412 to correct MD12-3412 oversampling is illustrated on the right side. Stratigraphic data are represented (MIS boundaries according to age model, positions of radiocarbon dates in red dots, Toba eruption in purple dots, and δ18O G.ruber pointers in black dots). Location of Figure 4 is shown. The grey rectangle corresponds to the core bottom unexploited here according to potential methane releases.

Figure 4: Example of turbidite sequences successions: Zr/Rb and Si/Al ratios, D50, grain size distribution, and Scopix radiography. Location of Figure 5 is shown.

Figure 5: Example of grain size excursion and detailed composition of bases in plane-polarised light (PPL) and cross-polarised light (XPL). d.: hemipelagic decantation, p.l.: planar lamination, b.: bioturbation, c.b.: coarser bed, c.l.: cross lamination, e.s.: erosional surface, m.f.: mud rich in forams. Planar laminations (Td), cross laminations (Tc), and erosional surfaces with decrease in grain size from erosional surface to decantation are typical of Bouma's sequences (Bouma, 1962).

Figure 6: Age model (black line) of the MD12-3412 core and associated sedimentation rate (dashed line). Radiocarbon dates are represented by red dots, Toba eruption is represented by a green dot, and $\delta^{18}O$ *G.ruber* pointers tuned on the revised template by Imbrie and Imbrie (1980) are represented by black dots.

Figure 7: Relation between turbidite occurrence and thickness, Indian monsoon, and global sea-level variability over the last 250 ka. Note that turbidites occurred during glacial sea-level low stands (grey bars), and do not follow the monsoonal trends.

Figure 8: Comparison between MD12-3412 (E4 channel; this study) and MD12-3417 (Active Valley; Fournier et al., 2017) controlling factors. The location of both cores is reported in Figure 1.

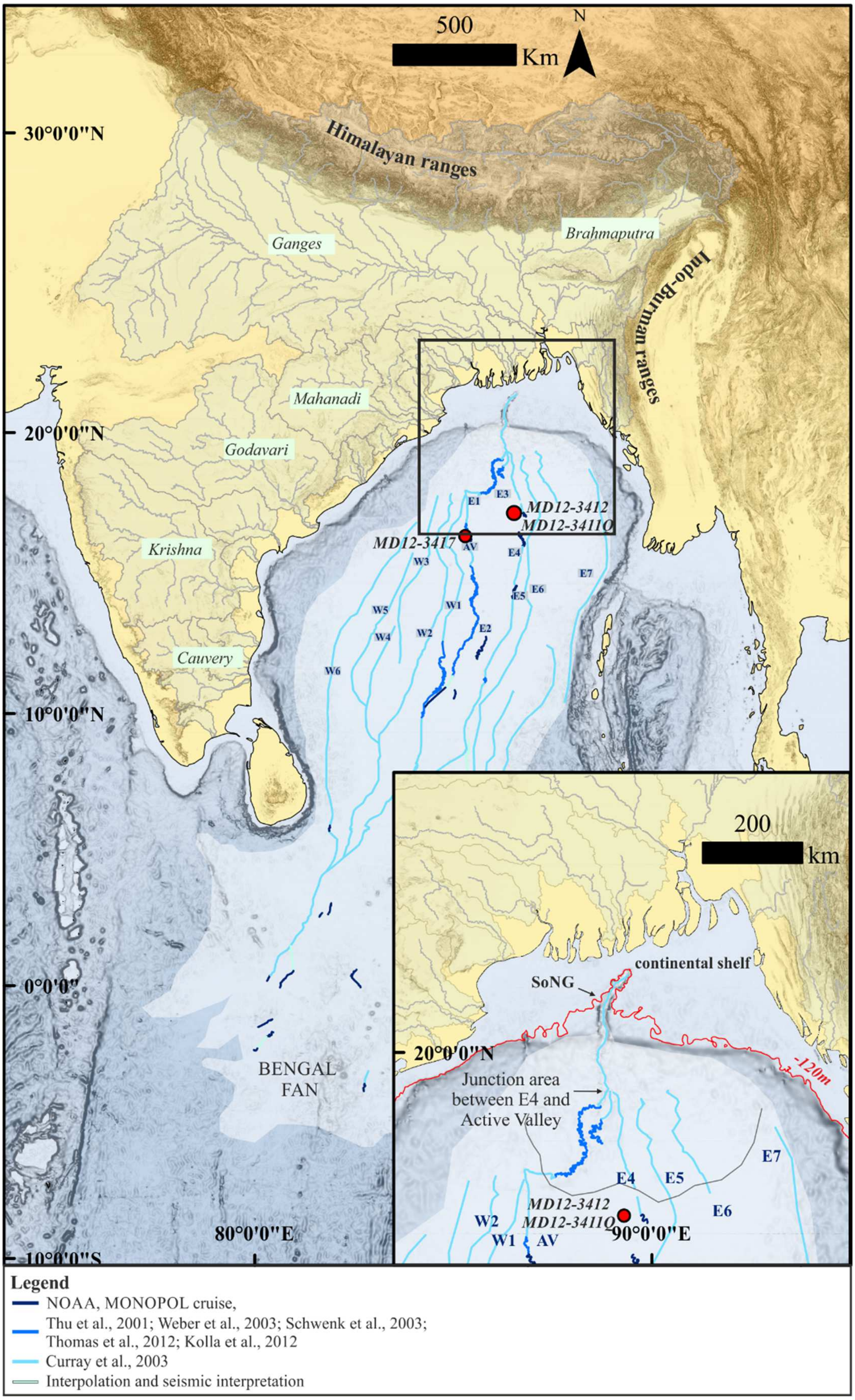
500
Km
N
30°0'0"N
Himalayan ranges
Ganges
Brahmaputra
Indo-Burman ranges
Mahanadi
Godavari
Krishna
Cauvery
20°0'0"N
10°0'0"N
0°0'0"
-10°0'0"S
80°0'0"E
BENGAL
FAN
MD12-3412
MD12-3411Q
MD12-3417
AV
E1
E2
E3
E4
E5
E6
E7
W1
W2
W3
W4
W5
W6
200
km
continental shelf
SoNG
20°0'0"N
-120m
Junction area
between E4 and
Active Valley
90°0'0"E
Legend
NOAA, MONOPOL cruise,
Thu et al., 2001; Weber et al., 2003; Schwenk et al., 2003;
Thomas et al., 2012; Kolla et al., 2012
Curray et al., 2003
Interpolation and seismic interpretation

Figure 1

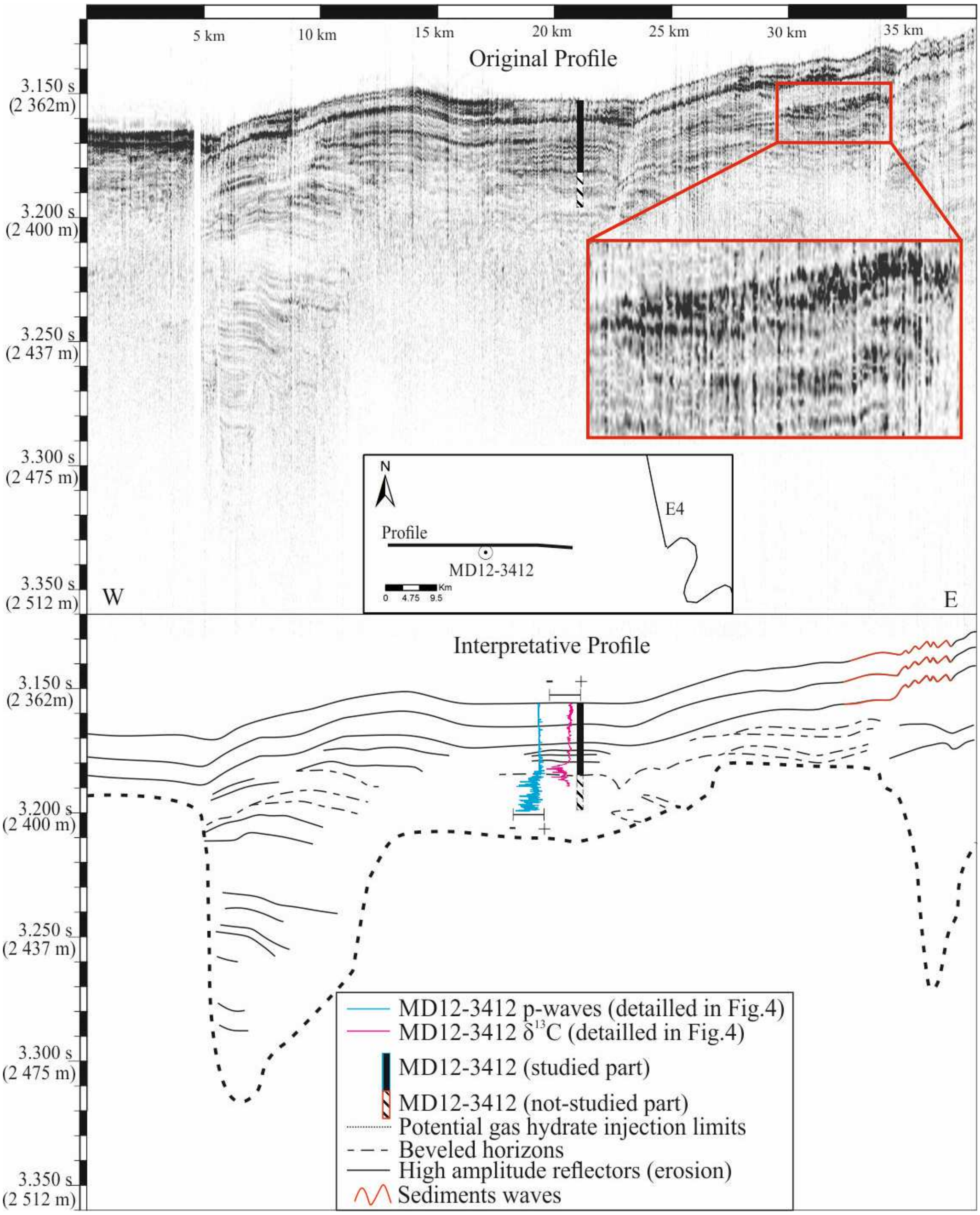

5 km
10 km
15 km
20 km
25 km
30 km
35 km
Original Profile
3.150 s
(2 362m)
3.200 s
(2 400 m)
3.250 s
(2 437 m)
3.300 s
(2 475 m)
3.350 s
(2 512 m)
W
E
N
Profile
MD12-3412
E4
Km
0
4.75
9.5
Interpretative Profile
MD12-3412 p-waves (detailled in Fig.4)
MD12-3412 δ13C (detailled in Fig.4)
MD12-3412 (studied part)
MD12-3412 (not-studied part)
Potential gas hydrate injection limits
Beveled horizons
High amplitude reflectors (erosion)
Sediments waves

Figure 2

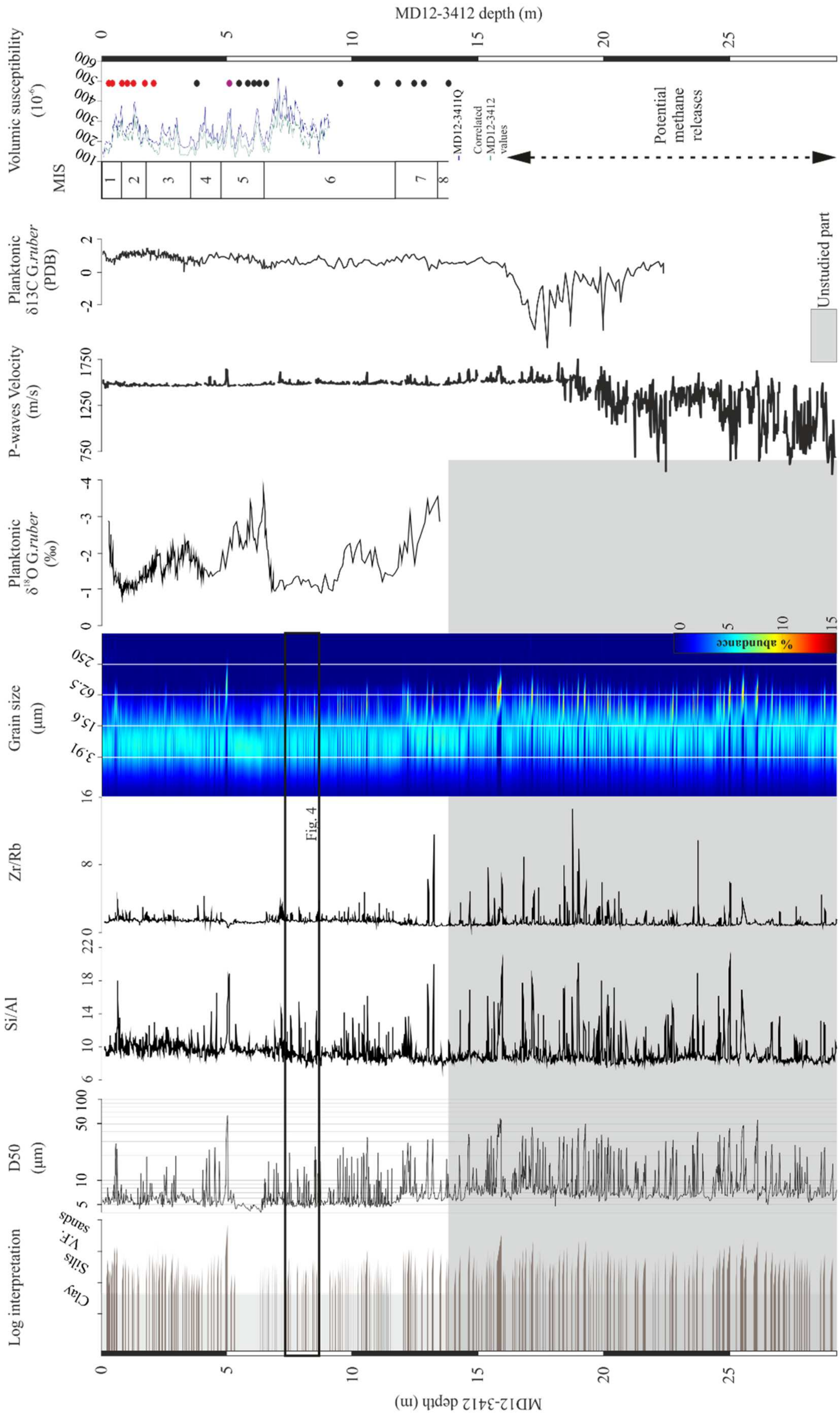

MD12-3412 depth (m)
Volumic susceptibility (10⁻⁶)
MIS
MD12-3411Q
Correlated MD12-3412 values
Potential methane releases
Planktonic δ13C G.ruber (PDB)
Unstudied part
P-waves Velocity (m/s)
Planktonic δ18O G.ruber (‰)
Grain size (µm)
% abundance
Fig. 4
Zr/Rb
Si/Al
D50 (µm)
Log interpretation
Clay
Silts
V.F. sands

Figure 3

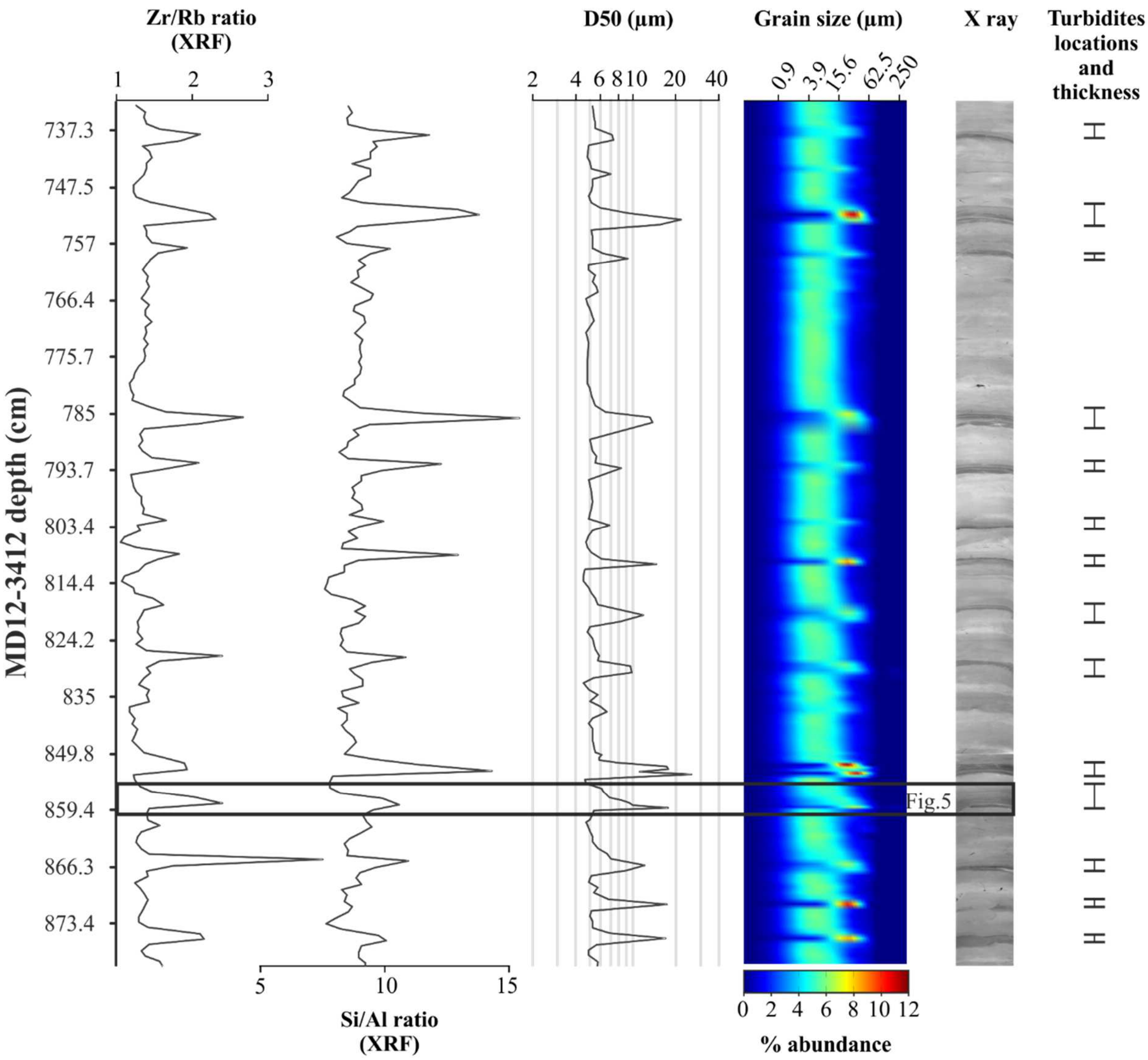

Zr/Rb ratio (XRF)
1 2 3
D50 (µm)
2 4 6 8 10 20 40
Grain size (µm)
0.9 3.9 15.6 62.5 250
X ray
Turbidites locations and thickness
MD12-3412 depth (cm)
737.3
747.5
757
766.4
775.7
785
793.7
803.4
814.4
824.2
835
849.8
859.4
866.3
873.4
Fig.5
5 10 15
Si/Al ratio (XRF)
0 2 4 6 8 10 12
% abundance

<u>Figure 4</u>

686

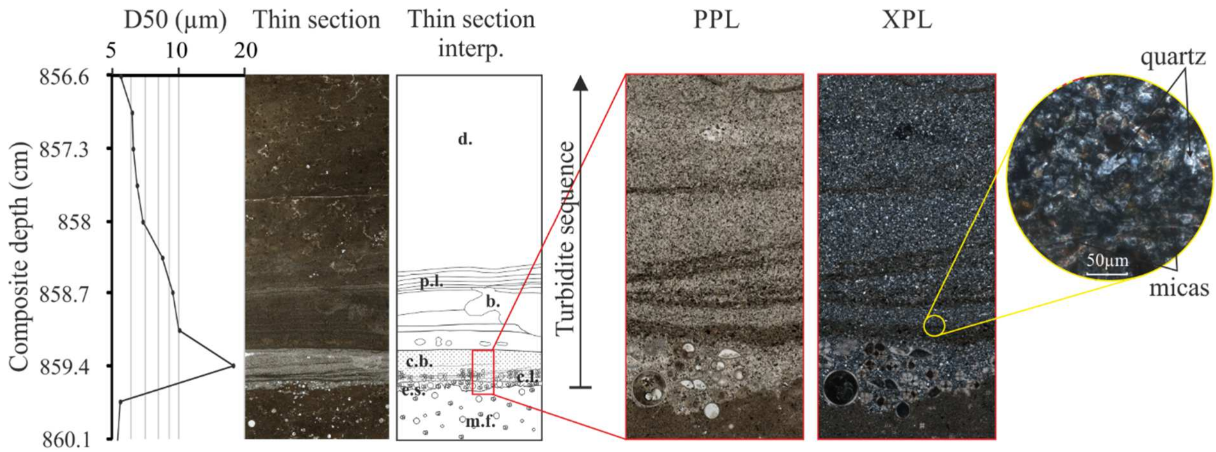

687 Figure 5

688

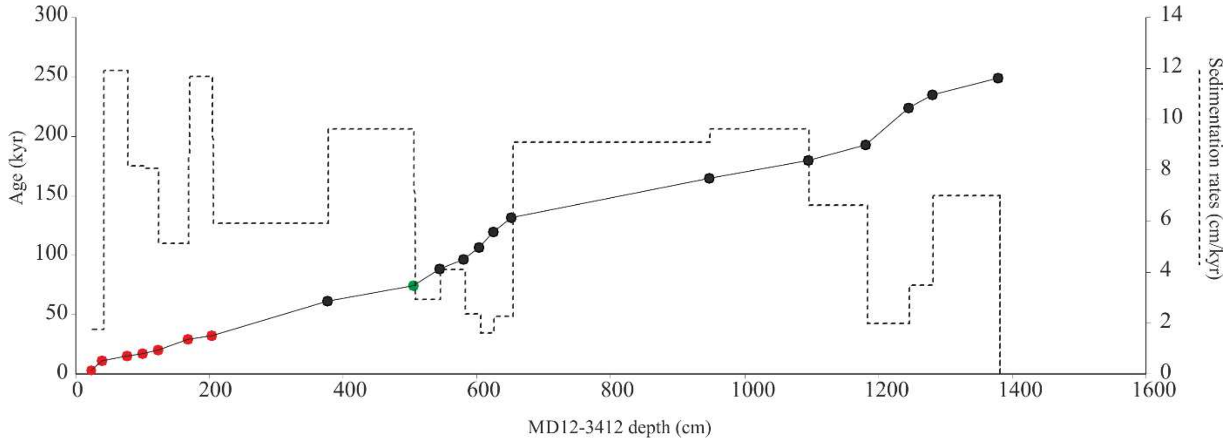
Age (kyr)
300
250
200
150
100
50
0
Sedimentation rates (cm/kyr)
14
12
10
8
6
4
2
0
0
200
400
600
800
1000
1200
1400
1600
MD12-3412 depth (cm)

<u>Figure 6</u>

692

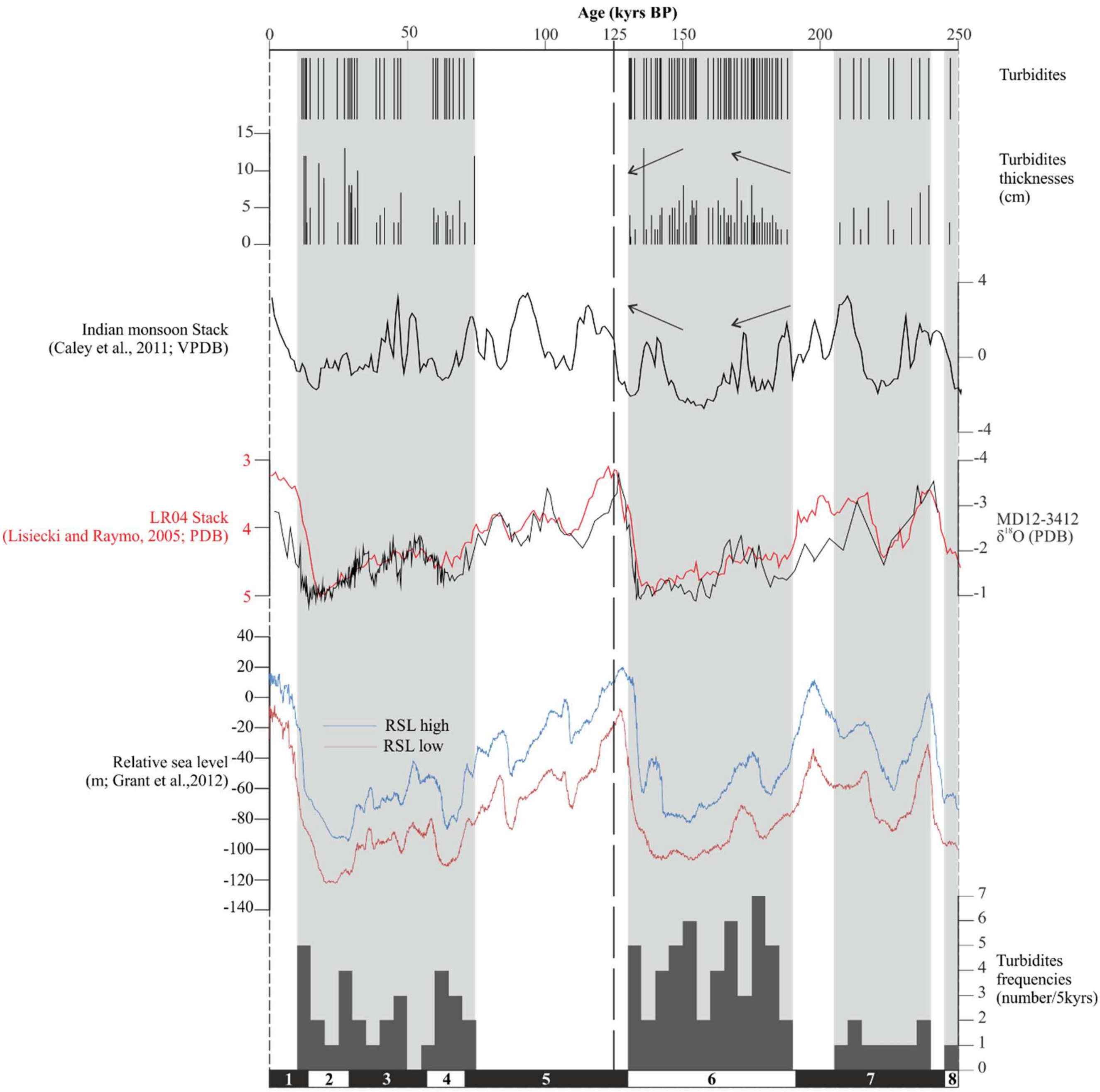

693 MIS (Lisiecki and Raymo, 2005)

694 Figure 7

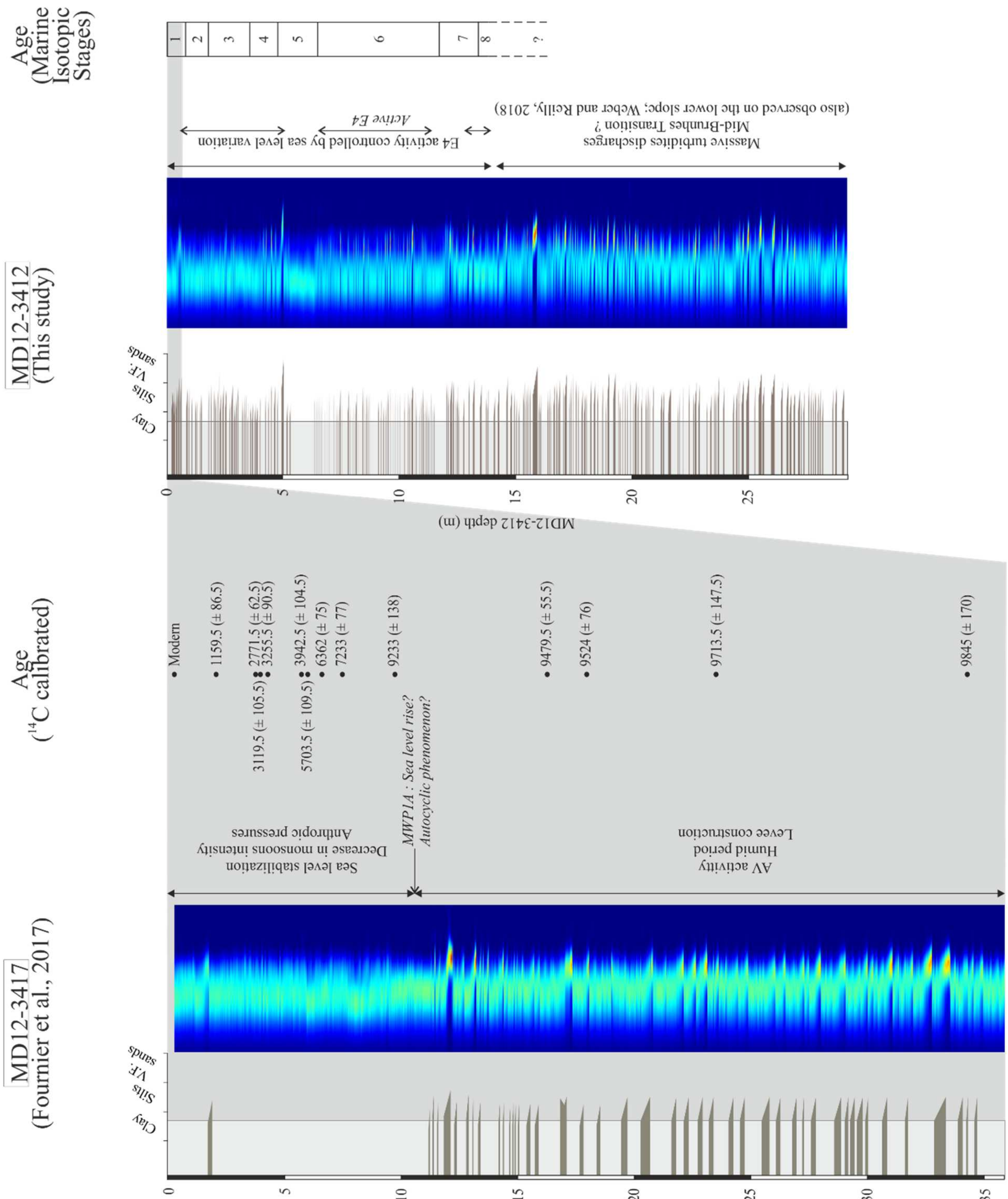

MD12-3417 (Fournier et al., 2017)
Age (14C calibrated)
MD12-3412 (This study)
Age (Marine Isotopic Stages)
Clay
Silts
V.F. sands
MD12-3417 depth (m)
MD12-3412 depth (m)
Sea level stabilization
Decrease in monsoons intensity
Anthropic pressures
MWP1A : Sea level rise?
Autocyclic phenomenon?
AV activity
Humid period
Levee construction
Modern
1159.5 (± 86.5)
3119.5 (± 105.5)
2771.5 (± 62.5)
3255.5 (± 90.5)
5703.5 (± 109.5)
3942.5 (± 104.5)
6362 (± 75)
7233 (± 77)
9233 (± 138)
9479.5 (± 55.5)
9524 (± 76)
9713.5 (± 147.5)
9845 (± 170)
E4 activity controlled by sea level variation
Active E4
Massive turbidites discharges
Mid-Brunhes Transition ?
(also observed on the lower slope; Weber and Reilly, 2018)

<u>Figure 8</u>